water

MDPI

Article

Multidisciplinary Observations across an Eddy Dipole in the Interaction Zone between Subtropical and Subantarctic Waters in the Southwest Atlantic

Eugene G. Morozov [1,2,*], Dmitry I. Frey [1,2], Victor A. Krechik [1], Aleksandr A. Latushkin [2], Pavel A. Salyuk [3], Anna M. Seliverstova [1], Sergey A. Mosharov [1], Alexei M. Orlov [1,4], Svetlana A. Murzina [1,5], Alexej V. Mishin [1], Pavel V. Chukmasov [4], Arseny A. Kubryakov [2], Maxim V. Budyansky [3], Oleg A. Zuev [1], Olga S. Mekhova [1], Vladimir I. Ponomarev [3], Anna L. Chultsova [1], Anna V. Masevich [2], Nadezhda I. Torgunova [1], Andrey O. Kholmogorov [3], Elena A. Shtraikhert [3], Irina V. Mosharova [1], Nikolay Yu. Neretin [1,6], Glafira D. Kolbasova [1,6], Vitaly L. Syomin [1], Andrey V. Tretiakov [4], Larisa G. Tretiakova [4] and Anton D. Chernetsky [1]

[1] Shirshov Institute of Oceanology, Russian Academy of Science, 36 Nakhimovsky pr., 117997 Moscow, Russia
[2] Marine Hydrophysical Institute, Russian Academy of Science, 2 Kapitanskaya ul., 299011 Sevastopol, Russia
[3] V.I. Ilichev Pacific Oceanological Institute, Far Eastern Branch of the Russian Academy of Science, 43 Baltiiskaya ul., 690041 Vladivostok, Russia
[4] Severtsov Institute of Ecology and Evolution, Russian Academy of Sciences, 33 Leninsky Prospekt, 119071 Moscow, Russia
[5] Institute of Biology of the Karelian Research Centre of the Russian Academy of Sciences, 11 Pushkinskaya Street, 185910 Petrozavodsk, Russia
[6] N.A. Pertsov White Sea Biological Station, Faculty of Biology, Moscow State University, 1 Leninskiye Gory, 119991 Moscow, Russia
* Correspondence: egmorozov@mail.ru

Abstract: Seawater properties in two intense rings in the South Atlantic are considered. One ring separated from the Brazil Current and the other from the Malvinas Current. The analysis is based on the CTD casts and SADCP measurements from the onboard velocity profiler. The optical properties, chemical parameters, methane concentration, and biological properties such as primary production, plankton, and fish were also analyzed. Analysis of strong differences between the eddies is supplemented by observations of whales and birds in the region.

Keywords: subtropical rings; Subantarctic rings; CTD; ADCP; optical and hydrochemical parameters; methane; primary production; plankton; fish; birds and whales

check for updates

Citation: Morozov, E.G.; Frey, D.I.; Krechik, V.A.; Latushkin, A.A.; Salyuk, P.A.; Seliverstova, A.M.; Mosharov, S.A.; Orlov, A.M.; Murzina, S.A.; Mishin, A.V.; et al. Multidisciplinary Observations across an Eddy Dipole in the Interaction Zone between Subtropical and Subantarctic Waters in the Southwest Atlantic. *Water* **2022**, *14*, 2701. https://doi.org/10.3390/w14172701

Academic Editor: Bruno Charrière

Received: 6 June 2022
Accepted: 22 August 2022
Published: 30 August 2022

Publisher's Note: MDPI stays neutral with regard to jurisdictional claims in published maps and institutional affiliations.

Copyright: © 2022 by the authors. Licensee MDPI, Basel, Switzerland. This article is an open access article distributed under the terms and conditions of the Creative Commons Attribution (CC BY) license (https://creativecommons.org/licenses/by/4.0/).

1. Introduction

Mesoscale eddies are very important elements of the global ocean circulation. Mesoscale eddies transport mass, momentum, heat, and freshwater over the basins of the ocean. They strongly influence the mean sate of the ocean and together with internal waves transport nutrients to the upper layer of the ocean. The energy of eddies exceeds that of the mean circulation by an order of magnitude, which was first reported during the Atlantic Polygon-70 experiment [1]. Eddies are generally formed due to the instabilities of the mean flow [2]. The most energetic frontal rings are formed due to meandering of the jet currents. Mesoscale rings are generated by finite-amplitude instabilities of currents, which result in the spreading of a volume of fluid into a region with different environmental characteristics [3]. It is clear that temperature and salt anomalies associated with these rings are important sources for the transformation of properties of water masses [3].

Two intense currents in the South Atlantic, the warm Brazil Current and cold Malvinas Current, form a confluence region at approximately 38–40° S [4,5]. An intense oceanic front exists between these two currents; rings of opposite sign are generated at the front

with intermediate water masses between rings. Thus, one of the most intense oceanic fronts appears that generates rings of opposite sign and forms intermediate water masses. The exchange of mass, heat, and salt between Subantarctic and subtropical waters leads to intense primary production and transformation of water properties [6]. The Malvinas Current is related to the Subantarctic Front (SAF) and the Brazil Current forms the Brazil Current Front (BCF). Some studies indicate that the SAF is organized in two branches [7,8] that merge further downstream at approximately 44° S [9]. In the confluence region the SAF and BCF converge to a single front, the Brazil–Malvinas Confluence Front (BMCF) [10]. Confluence of the Malvinas and Brazil currents forms a strong front that generates many rings and eddies. After the collision, the Malvinas Current turns back to the south as the Malvinas Return Flow [11]. The retroflection of the Malvinas Current and continuation of the Brazil Current results in meandering and formations of rings, eddies, and filaments [12]. It is noteworthy that eddy advection has an important effect on the variability of the Atlantic meridional overturning circulation (AMOC) on different time scales [13–15]. Some publications report a strong influence of eddies on the cross-shelf transport of fresh river water from the coast of Brazil in the BMCF region, which can cause sharp changes in the salinity in the study region [11,16].

The studies of the BMCF included CTD surveys and moorings [17], satellite data [18], and modeling [19,20]. A new approach to studying the propagation of eddies was suggested in [21], which involved applying observations of the motion of loggerhead sea turtles to trace mesoscale eddies. Unfortunately, there are very few in situ measurements of the vertical structure of eddies in the study region. One of the rare exceptions is the publication by Gordon [11], in which the data are presented on the thermohaline structure of two anticyclones and one cyclone in the BMCF. The authors showed that a significant modification of the characteristics of water masses occurs in eddies. In particular, it was shown that intense winter mixing in the cores of anticyclones leads to the penetration of salty and cold waters into their lower layers.

Lentini et al., [22] analyzed the statistics of warm-core rings formed in the Brazil–Malvinas Confluence region based on a continuous time series of satellite data from January 1993 to December 1998. On average, seven rings per year were released into Subantarctic waters. The lifetime of the rings ranged from 11 to 95 days, with a mean value of 35 days. These rings were mostly elliptical anticyclonic rings with a mean major radius of 126 $\pm$ 50 km and a minor radius of 65 $\pm$ 22 km, and with translation speeds ranging from 4.2 to 27.2 km per day (4.8–31.5 cm/s). None of them seemed to remain more than 4 months in the confluence region.

Lentini et al., [23] analyzed rings of the Brazil Current. They report that warm-core anticyclonic rings were shed by the meander of the current after poleward excursions of the Brazil Current. Approximately one ring is formed by the current in 2 months. The observed lifetime ranges between 1 and 4 months, with a mean value of approximately 2 months. Two or three anticyclonic rings of the Brazil Current were observed to coexist in the confluence region. Most of the rings were moving to the south. The mean horizontal scale of the eddies was 55 km; and mean translation speed was 10 km per day [23].

Mason et al., [24] report on the basis of altimetry data that motions associated with mesoscale eddies and meanders are responsible for significant transports of mass and heat. Mesoscale vertical fluxes also influence upper ocean biological productivity by transporting nutrients into the euphotic layer. They estimated that the maximum eddy lifetime in the region varies from 78 to 198 days.

Mason et al., [24] distinguish the following eddy properties: amplitudes, radii, intensity, and nonlinearity. Eddy intensity is the ratio between the eddy amplitude and its radius, A/Ls [25]. Eddy nonlinearity is the ratio between eddy swirl speed and translation velocity, U/c [26]. Eddy intensities generally range from zero to 0.5, while eddy nonlinearity varies from zero to 15. Eddy intensity and nonlinearity are greater in cold cyclones. We emphasize that strong currents exist at the boundary between cyclones and anticyclones. The eddy radii of cyclones based on altimetry data in Mason et al., [24] varies from 69 km in the

region at 45° S to 75 km in the northern region (~35° S). The radii of anticyclones vary from 90 to 62 km. The amplitudes do not have a clearly pronounced regularity and vary from 38 to 9 cm; the amplitudes of anticyclones are generally smaller. The swirl speed is generally greater in cyclones and varies from 58 to 17 cm/s. Propagation velocity varies from 0.5 to 8.8 cm/s.

Studies of variations in biooptical characteristics in the eddy zone of the Southwest Atlantic have been carried out mainly using satellite ocean color imaging [12,21,27,28]. In these works, the surface distribution of remotely determined chlorophyll-a in anticyclonic and cyclonic eddies was mainly considered, and there are almost no works that analyze a wider number of biooptical characteristics, and also do not consider the features of their vertical distribution. At the same time, with the help of multidisciplinary analysis of biooptical and other oceanographic characteristics, a more detailed study of physical and biological processes in the eddy structures is possible.

Despite numerous above-mentioned papers dedicated to studies of eddies in the Southwest Atlantic, there is still no available data on synchronous measurements of physical, optical, chemical, and biological properties of waters within eddies of different polarity in this region. The main goal of this multidisciplinary study is to trace changes in water properties between the waters of the subtropical and Subantarctic origin, which are observed in anticyclonic and cyclonic eddies, respectively. With this in mind, we selected an eddy dipole based on satellite altimetry data and performed measurements at seven stations along a section across the rings connecting their centers (Figure 1).

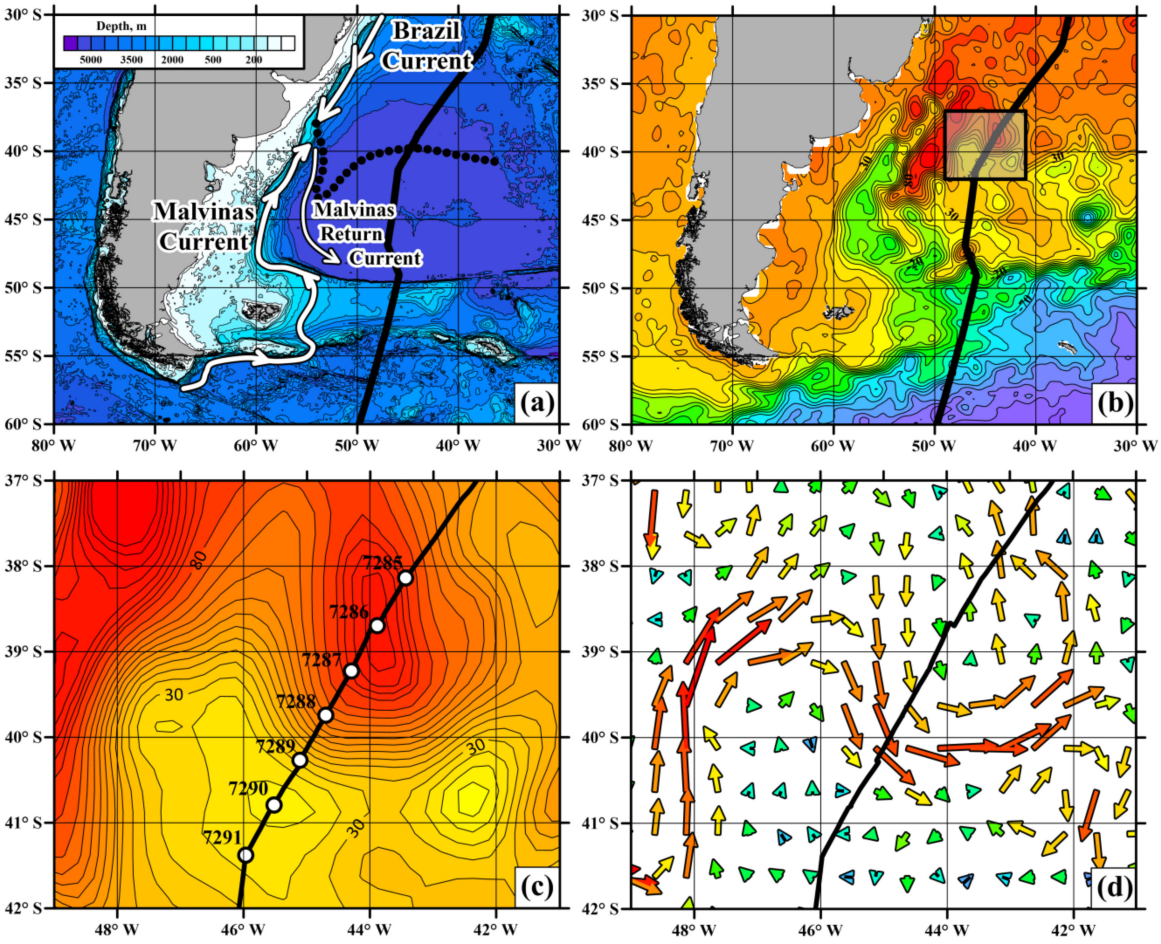


Figure 1. Location of measurements on 11–13 January 2022. Panel (**a**): schematic of the surface circulation in the Southwest Atlantic. The location of the Brazil–Malvinas Confluence zone is shown

by dotted line; the main surface currents are indicated by white arrows. Bottom topography is shown based on the GEBCO database [https://www.gebco.net/data_and_products/gridded_bathymetry_data/gebco_2021] (access date 21 August 2022); the shoreline is shown based on the GSHHS data [29]. Panel (**b**): Absolute dynamic topography (ADT) map at the time of in situ measurements (10 January 2022). Gray rectangle indicates the limits of maps (**c**,**d**). Panel (**c**): detailed ADT map in the region of rings. White dots indicate the location of CTD stations. Panel (**d**): sea surface altimetry-derived geostrophic circulation on 10 January 2022. Solid black line denotes the ship route on all panels.

2. Data and Methods

This study is based on the multidisciplinary data linking physical and biological processes in a pair of cyclonic and anticyclonic rings near the BMC zone in the Southwest Atlantic. In this section, we describe our approach for the selection of rings for our measurements based on satellite altimetry data (Section 2.1), present Lagrangian simulation methods for studies of water origin (Section 2.2), discuss measurements of thermohaline eddy structure together with its velocity field based on CTD and SADCP measurements (Section 2.3), describe the measurements of optical water properties (Section 2.4), and the biological studies of waters within selected eddies (Sections 2.5–2.7).

The measurements over the section across two rings were carried out on 11–13 January 2022; seven stations of CTD profiling were occupied with an AML probe up to 500 m. water sampling with Niskin bottles was performed up to 200 m. According to the altimetry data and the data of the survey, the section crossed two rings: with warm waters from the warm Brazil and cold Malvinas currents. Their centers were at stations 7286 (Brazil Current ring) and 7290 (Malvinas Current ring). Stations 7285, 7287, 7289, and 7291 were peripheral, and station 7288 was in the mixing zone.

2.1. Satellite Altimetry Data

In this work, we used satellite altimetry data for selection of a section between the centers of the cyclonic and anticyclonic eddies and locations of stations along the section. We used the Data Unification and Altimeter Combination System (DUACS) near real time altimeter gridded product of 0.25° [30] available from Copernicus Marine Environment Monitoring Service (CMEMS, http://marine.copernicus.eu/ (accessed on 15 February 2022)). This product includes the data from all available altimeters and consists of the absolute dynamic topography (ADT), sea level anomalies (SLA), surface-geostrophic velocities, and surface-geostrophic velocity anomalies, which are sampled daily on a Mercator regular grid. Thus, we can estimate the location of eddy centers with an accuracy of 0.25°, which corresponds to 28 km in the meridional direction and 21 km in the zonal direction at this latitude (40° S).

2.2. Lagrangian Analysis

Lagrangian analysis has been applied to study the origin of waters in the study area, in which geostrophic current velocities calculated from the AVISO satellite altimetry data ($0.25 \times 0.25°$) were used to calculate particle trajectories. A large number of synthetic particles (the area shown in Figure 2 has been seeded daily with tracers on a grid of 700×700 points) and their trajectories have been computed back in time for a fixed period of time [31]. The back-in-time integration period in our study is two years. One obtains an origin Lagrangian map (O-map) by marking the particles with different colors, which arrived from the northern, western, southern, and eastern boundaries of the study area in the past. The origin Lagrangian maps were computed daily on 11–13 January 2022.

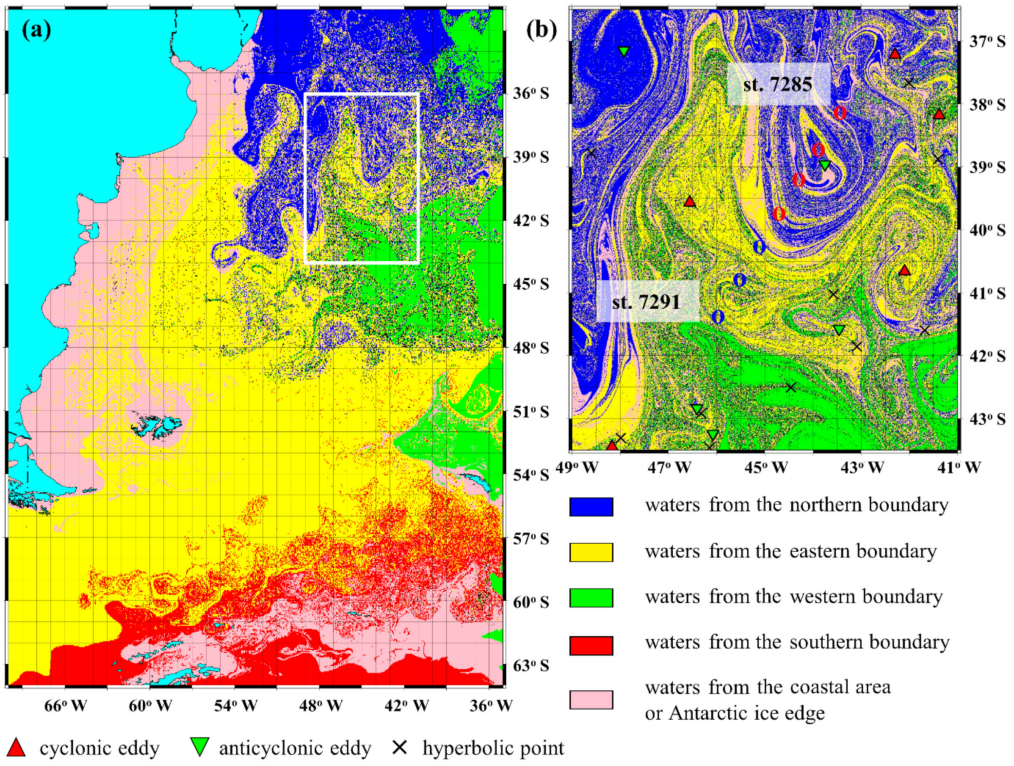


Figure 2. (**a**,**b**) shows the backward-in-time Lagrangian origin map on 12 January 2022. Blue color denotes water particles from the northern edge of the map from the subtropical region, yellow color denotes waters from the western edge of the map from the Drake Passage, red color denotes water from the southern edge of the map (Antarctica), green color denotes water from the eastern border of the map. Pink color denotes water particles that "touched" the shore or Antarctic ice edge and spread from the shore or the edge.

2.3. SADCP, CTD, and Hydrochemistry Data

Direct velocity measurements were carried out from the R/V *Akademik Mstislav Keldysh* (R/V AMK) equipped with an SADCP system Teledyne RD Instruments Ocean Surveyor (TRDI OS) with a frequency of 76.8 kHz. During the survey the profiler was set in the narrowband mode, which increases the profiling range up to 700 m depth. We set 60 vertical bins 16 m each with an 8 m blank distance immediately below the transducer. The draught of the ship is 6 m, which gives 22 m depth for the center of the first bin (the depth of the uppermost layer of velocity measurements). Time averaging of the raw data was made over 120 s intervals. Since the ship speed varied between 8 and 10 knots, this time average represents an along-track averaging of roughly 500 m. Measurement errors in the amplitude of the horizontal velocities were small, approximately 1–2 cm/s [32]. The TPXO9 model [33] was used to subtract the barotropic tidal velocities at the moment of measurements. Typical tidal velocities in the region are less than 2–3 cm/s which is insignificant for the high-velocity jets at the periphery of the rings.

The CTD data were collected at seven stations performed from the sea surface to 500 m depth (Table 1). An AML Oceanographic BaseX CTD probe was used for these measurements. Sampling rate was set to 4 Hz, the CTD vertical speed was 1 m/s, which gives the initial vertical resolution equal to 0.25 m. Only downcast data were used as the CTD profile data. The standard SeaCast software (Version 4.4.0) (software was supplied with the purchased instrument from SBE-electronics Inc. Bellevue, USA) was used for the data collection.

Table 1. Location, time, and type of measurements at seven stations between centers of cyclonic and anticyclonic rings in the Southwest Atlantic performed on 11–13 January 2022.

No. st.	Date/Time (UTC)	Coordinates	CTD Depth, m	Type of Measurements
7285	11 January 2022, 12:22	38°08.3′ S, 43°26.2′ W	500	CTD, Optics, Niskin bottles (0, 15, 70, 110, 200, 500 m)
7286	11 January 2022, 18:42	38°41.7′ S, 43°53.2′ W	500	CTD, Optics, Double square net (DSN), Niskin bottles (0, 15, 40, 80, 130, 150, 200, 500 m)
7287	12 January 2022, 02:16	39°13.3′ S, 44°17.8′ W	500	CTD, Optics, Niskin bottles (0, 20, 60, 83, 130, 200, 500 m)
7288	12 January 2022, 08:40	39°44.7′ S, 44°42.3′ W	500	CTD, Optics, Niskin bottles (0, 30, 45, 73, 110, 200, 500 m)
7289	12 January 2022, 15:23	40°16.4′ S, 45°06.4′ W	500	CTD, Optics, Niskin bottles (0, 18, 40, 70, 110, 200, 500 m)
7290	12 January 2022, 21:55	40°47.6′ S, 45°31.1′ W	500	CTD, Optics, DSN, Niskin bottles (0, 15, 40, 60, 100, 200, 500 m)
7291	13 January 2022, 06:05	41°22.8′ S, 45°58.3′ W	500	CTD, Optics, Pleiston net, Niskin bottles (0, 18, 45, 70, 200, 500 m)

Water samples for chemical analysis and methane were taken from the Niskin bottles to 200 m. The contents of the main forms of nutrients were determined: inorganic forms of silicate, mineral phosphorus, nitrate, nitrite and ammonium nitrogen, as well as dissolved oxygen, total alkalinity (*Ta*) and pH. Further processing of samples for the study of all these parameters was carried out in the onboard laboratory immediately after sampling.

The "HeadSpace" equilibrium concentration method [34] was used to analyze the methane content. The gas chromatograph Crystal Lux 4000 was used. Calculation of dissolved methane concentration in seawater was performed using the method described in [35] and modified in [36] using the calculated methane solubility constants.

2.4. Biooptical Measurements Using a Hydro-Optical Profiler

Biooptical measurements were carried out to the depths of 250 m using a complex of profiling hydrooptical equipment, consisting of Turner C6P and Kondor meters (manufactured by Akvastandart-Yug, Sevastopol, Russia, http://ecodevice.com.ru/ecodevice-catalogue/multiturbidimeter-kondor, accessed on 1 December 2021). Chlorophyll-a (Chl-a) and colored dissolved organic matter (CDOM) fluorescence intensity measurements were performed using a Turner C6P instrument. The Kondor probe determined the attenuation index of directional light at 660 nm (BAC660) and photosynthetically active radiation (PAR). BAC660 in the red band of the spectrum was determined from the absorbing and scattering properties of the total suspended matter (TSM); it depends on the CDOM absorption [37]. The PAR measurements were made only during daylight hours.

The fluorescence intensities CDOM (FCDOM) were calibrated to the quinine sulfate units (QSU) under laboratory conditions just before the expedition. Chl-a fluorescence intensities were recalculated into mass concentrations of Chl-a ($C_{chl\text{-}a}$, μg/L) based on the results of standard measurements by the extract method in water samples [38] taken synchronously with hydrooptical profiling. Calibration of the BAC660 was carried out in the laboratory before the expedition based on the results of measurements in suspension solutions of formazin with a given concentration (FTU units).

2.5. Primary Production

Water samples were taken from five depths within the euphotic layer (0–80 m), where the levels of illumination allow photosynthesis. To assess the primary productivity of phytoplankton, the following parameters were determined: the rate of primary produc-

tion, potential photosynthetic activity, and the concentration of the main phytopigment chlorophyll "a".

The rate of primary production was determined experimentally using the radiocarbon method [39] by simulating light and temperature conditions using the original laboratory phyto-incubator developed by the authors with adjustable LED illumination. Subsamples were exposed for 3 h, then filtered through Vladipor membrane filters (0.45 μm). The radioactivity of the stock solution and filters was determined using a Triathler liquid scintillation counter (Hidex, Finland). The assimilation number (AN, specific primary production, mg C/mg chl/h) was calculated by normalizing the value of primary production at individual depths based on the corresponding concentration of chlorophyll "a". Chlorophyll "a" concentration in water was measured by the acetone extract fluorescence method [38].

Active fluorescence of chlorophyll "a" was measured using an ultrasensitive PAM fluorometer WATER-PAM (Walz, Germany). To estimate the current state of phytoplankton and its adjustment to light, the "fast light curves" method was used, according to which the effective quantum yield of phytoplankton photosystem II (PPSII) is measured and the relative electron transport rate in photosystem II (rETR) is calculated as a function of illumination [40,41]. The rETR value reflects the rate of conversion of light energy captured by chlorophyll "a" into chemically bound energy in phytoplankton cells, which provides the processes of biosynthesis of organic matter by phytoplankton. Photosynthetic efficiency reflecting the extent of use of the light energy in organic matter synthesis can be expressed through the ratio between AN and rETR values.

2.6. Fish and Invertebrates

Materials on fish and invertebrates were collected using a pelagic double square micronekton net (DSN) with an inlet area of 1 m^2 and a 6 m long filter cone made of gas with a mesh size of 0.5 mm [42], equipped with a water flow counter (Hydrobios, Germany) and a pterygoid deepener weighing 24 kg (Hydrobios, Germany). Oblique catches were carried out in the 600–0 m layer at a vessel speed of 2 knots. The hauling depth was determined based on the pressure sensor of the Senti DT probe (StarOddi, Iceland) readings. Samples were fixed in 2% formaldehyde solution, followed by transfer in 24 h to 96% ethanol. The species identification of ichthyoplankton was based on available data in the literature [43–48].

2.7. Sea Birds and Mammals

On-board ship observations of marine mammals and birds were performed in the study site. The observations were carried out continuously during the daylight hours at winds (Beaufort scale < 5) and visibility more than 50 m by two observers simultaneously from the port and starboard sides of the vessel from the direction-finding deck located at a height of 17 m above the sea level. The birds were detectable approximately 300 m from the ship.

3. Results

The data collected during the survey on 11–13 January 2022 in the Southwest Atlantic revealed the existence of a strong front between the relatively warm and saline subtropical waters within the anticyclonic eddy and cold and fresh Subantarctic waters within the cyclonic eddy. The physical, optical, chemical, and biological properties of these waters were studied along the transect between centers of the eddies. The results of these multidisciplinary measurements are presented separately below for each subject.

3.1. Origin of Waters within the Eddy Dipole

Figure 2 shows the backward-in-time Lagrangian origin map on 12 January 2022, which highlights the considered pair of interacting rings of opposite vorticity (Figure 1b). Similar methods of Lagrangian analysis were used in [49,50]. It can be seen that waters of various origins are involved in the rings, namely, subtropical (blue), Subantarctic (yellow),

as well as waters from the South American shelf (pink). The anticyclonic ring (in the figure, the centers of anticyclones are marked with green triangles) contains mainly waters of subtropical origin, and the cyclonic eddy (the centers of cyclones are marked with red triangles) contains Subantarctic waters.

3.2. SADCP and CTD Measurements and Chemistry

Thermohaline structure of the eddy dipole was studied based on CTD measurements at seven stations along a section connecting centers of the cyclonic and anticyclonic eddies (Figure 3; the locations of stations are shown in Figure 1 and Table 1). The second (station number 7286) and sixth (station number 7290) stations were made exactly at the centers of the eddies; the rest stations were made at a constant distance of 70 km (38 nm) from each other. All CTD measurements were performed from the sea surface to 500 m depth.

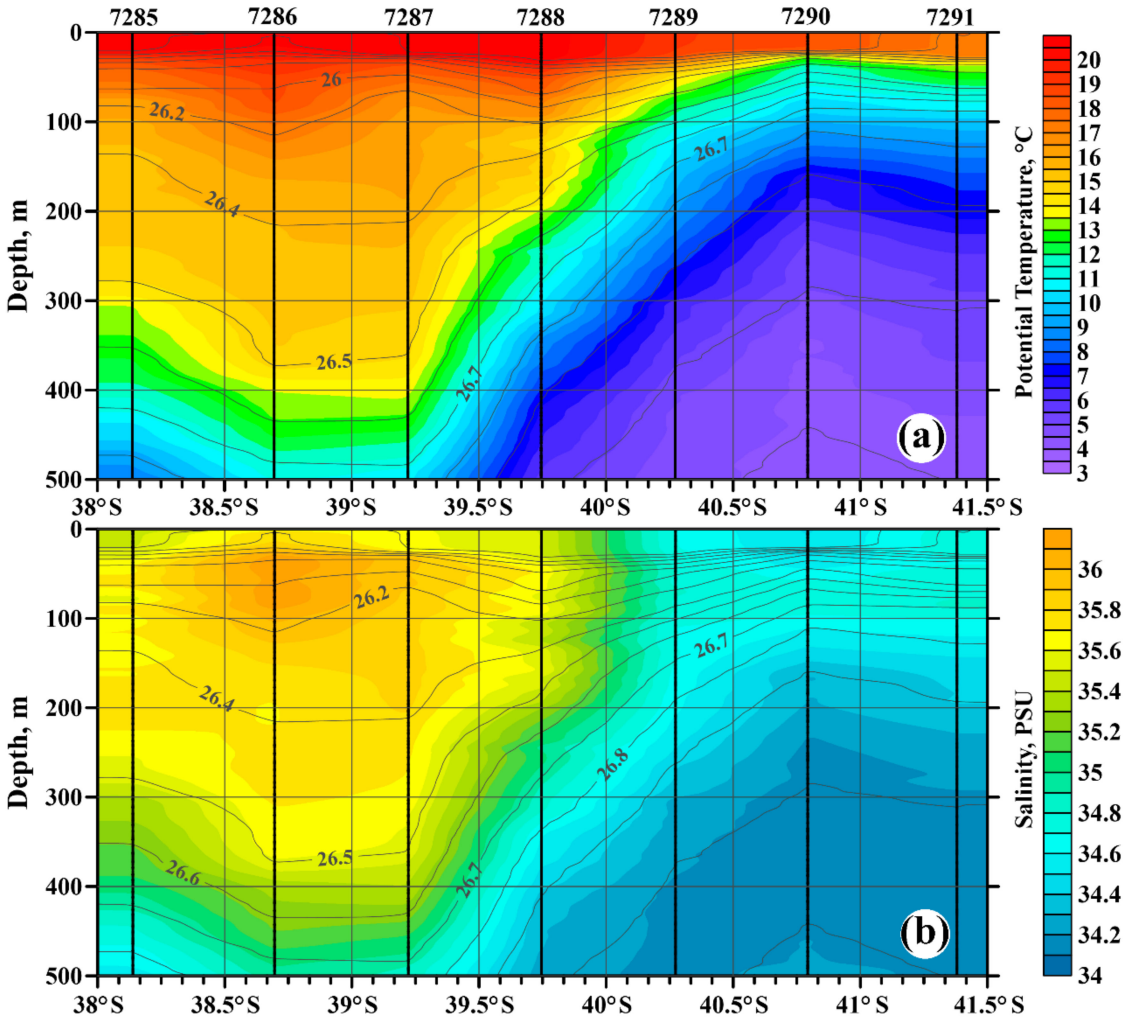


Figure 3. Sections of potential temperature (**a**) and salinity (**b**) across the rings based on CTD measurements. Isolines of potential density anomalies are shown by solid lines. Locations of stations are shown by thick black lines.

Distributions of potential temperature and salinity (Figure 3) show significant difference in properties of subtropical and Subantarctic waters. Thus, the potential temperature at 100 m depth changes from 17.6 °C (station 7286, subtropical waters, center of anticyclonic eddy) to 9.6 °C (station 7290, Subantarctic waters, center of cyclonic eddy) while the salinity changes from 36.02 PSU to 34.67 PSU. Corresponding differences are observed at all measured depths; for example, the changes at a depth of 500 m are from 11.1° to

4.3 °C and from 34.97 PSU to 34.23 PSU. The depth of 12 °C potential temperature isotherm changes from 468 m in subtropical waters to 37 m in Subantarctic waters. Note that the thermohaline structure of the upper 30 m ocean layer is not affected by the influence of subtropical and Subantarctic waters. This layer is warm and relatively fresh in comparison with deep layers of the ocean. The stratification is defined by temperature distribution; the pycnocline is observed at 25–35 m depending on a station. The thickness of the mixed ocean layer is almost the same within the cyclonic and anticyclonic eddies.

The θ,S-diagrams were analyzed from the data of seven stations along the section through the eddy dipole (Figure 4). Intense transformation of water masses takes place in the eddies. Saline surface tropical waters (TW) accumulate in anticyclones. They are differently grouped in the upper and lower parts of the water column. As a result, waters of almost uniform salinity (S = 35.5–36.0 PSU) with a temperature of 15–20 °C appear. Anticyclones contribute to the transfer of salt to the lower layers of water, as a result of which salty and relatively cold waters form in their lower part. Such conditions are favorable for the formation of salt fingers [11], which transport saline waters to the deep part and the salinization of South Atlantic Central Water (SACW).

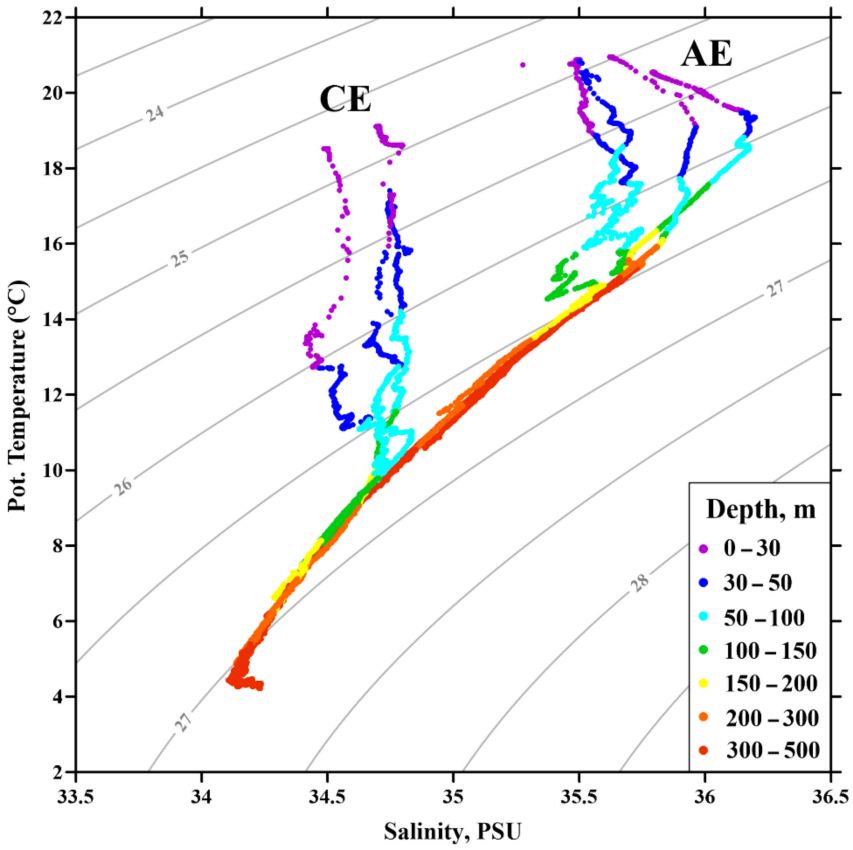


Figure 4. θ,S-diagram based on data from seven stations through an eddy dipole. The depth of measurements is shown with colors. CE is cyclonic eddy; AE is anticyclonic eddy.

Fresher SACW waters in cyclones ascend to the surface. They become warmer and mix with the tropical waters under the influence of the wind. As a result, relatively fresh waters with salinity (S = 34.5–34.7 PSU) are formed; their temperature varies from 10 °C to 18 °C, which is similar to the data reported in [11] for the Cleopatra eddy. In the upper part of the cyclones, due to the warming of fresh waters, waters of very low density appear and stratification increases, strongly blocking the vertical exchange (Figure 4).

The CTD stations were accompanied by along-track SADCP measurements (Figure 5). Measured velocities were projected to a direction of 120° (East-south-east), which corresponds to the direction of maximum velocity at the periphery of the eddies. This periphery

is organized in a form of two main high-velocity jets. They are located at a distance of 73 km from each other; maximum velocity of 84 cm/s in the first jet (40.2° S) is located at the sea surface while the second jet (39.4° S) with maximum velocity of 71 cm/s is located at a depth of 165 m. Velocities near the centers of the eddies are much lower and do not exceed 20 cm/s.

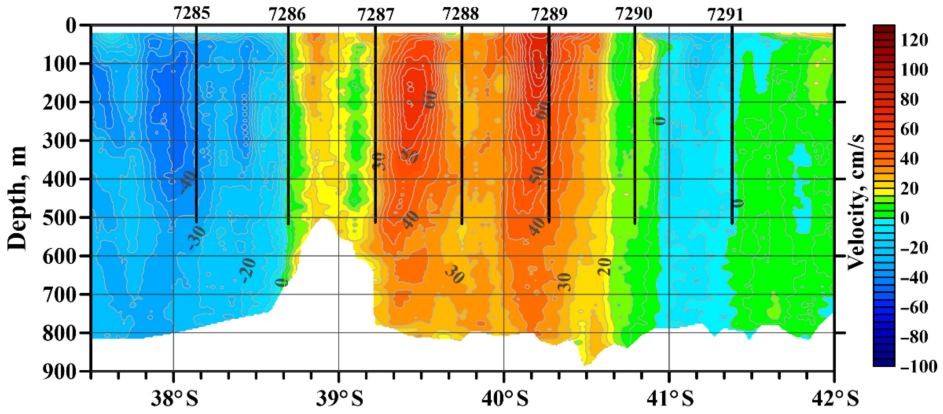


Figure 5. Velocity section across the rings based on SADCP measurements. Locations of stations are shown by thick black lines.

Three types of water can be clearly distinguished over the section: waters of two rings with different hydrochemical parameters and pronounced centers and a zone of their mixing. The warm ring of the Brazil Current is characterized by low concentrations of oxygen and nutrients as well as an increased total alkalinity. The cold ring of the Malvinas Current is characterized by high oxygen content and nutrients such as dissolved silicates, phosphorus and nitrates (Figures 6–9).

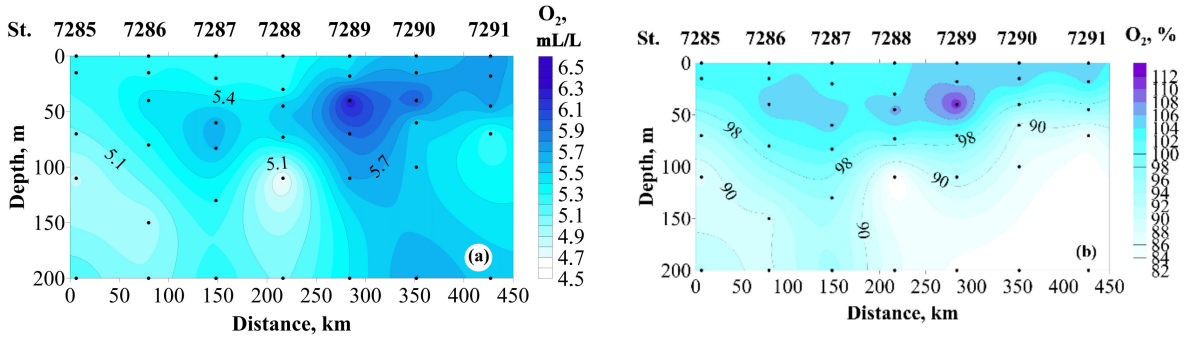


Figure 6. Concentration of dissolved oxygen (O_2, mL/L) (**a**) and degree of oxygen saturation (**b**) over the section.

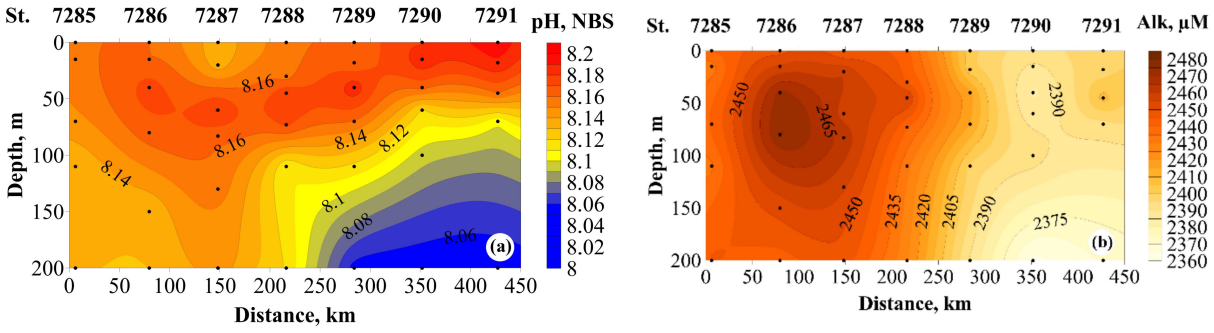


Figure 7. Distribution of pH (pH, NBS units) (**a**) and total alkalinity (Alk, µM) (**b**) over the section.

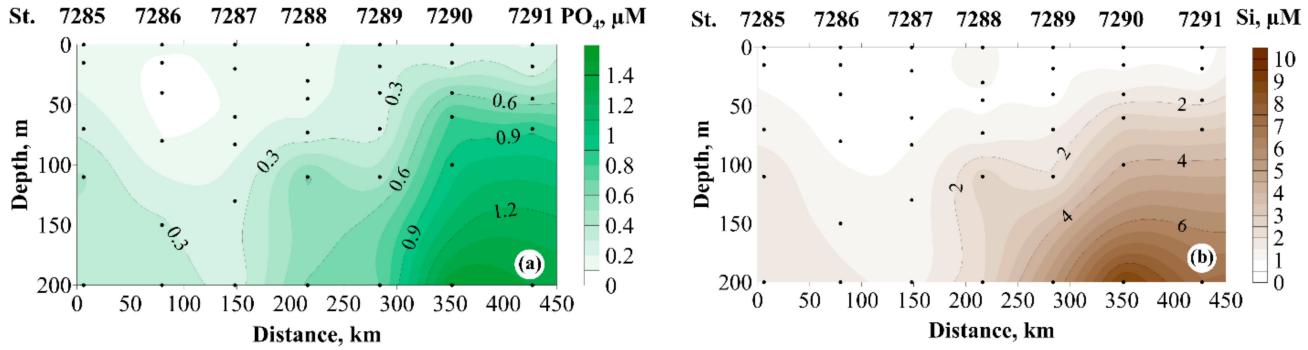


Figure 8. Distribution of dissolved phosphorus (PO_4, µM) (**a**) and silicates (Si, µM) (**b**) over the section.

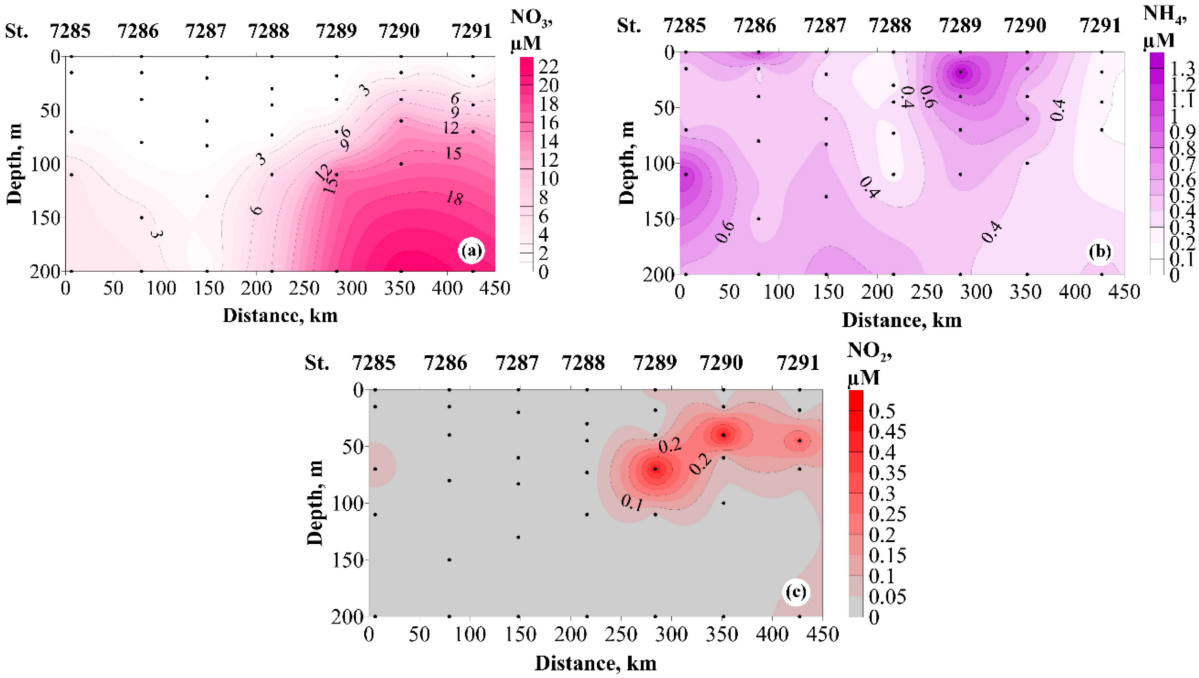


Figure 9. Distribution of nitrates (NO_3, µM) (**a**), nitrites (NO_2, µM) (**b**), and ammonium nitrogen (NH_4, µM) (**c**) over the section.

3.3. Methane Concentration in the Rings

We detected significantly different methane concentrations in the anticyclonic and cyclonic rings, as well as between them. In the anticyclonic ring, the average concentrations of methane are lower than in the cyclonic ring.

Medium (4.5–6 nM/L) and high (6–12.9 nM/L) methane concentrations were observed in the layer 2–200 m, and low (2.8–4.5 nM/L) between 200 and 500 m (Figure 10). Lower methane concentrations were observed in the central parts of the cyclonic (up to 3.8 nM/L at station 7290) and anticyclonic (up to 2.8 nM/L at station 7286) rings at a depth of 200 m and 500 m, respectively. The maximum concentration of methane (12.9 nM/L) was observed at the central station 7288 of the section between the rings at a depth of 110 m.

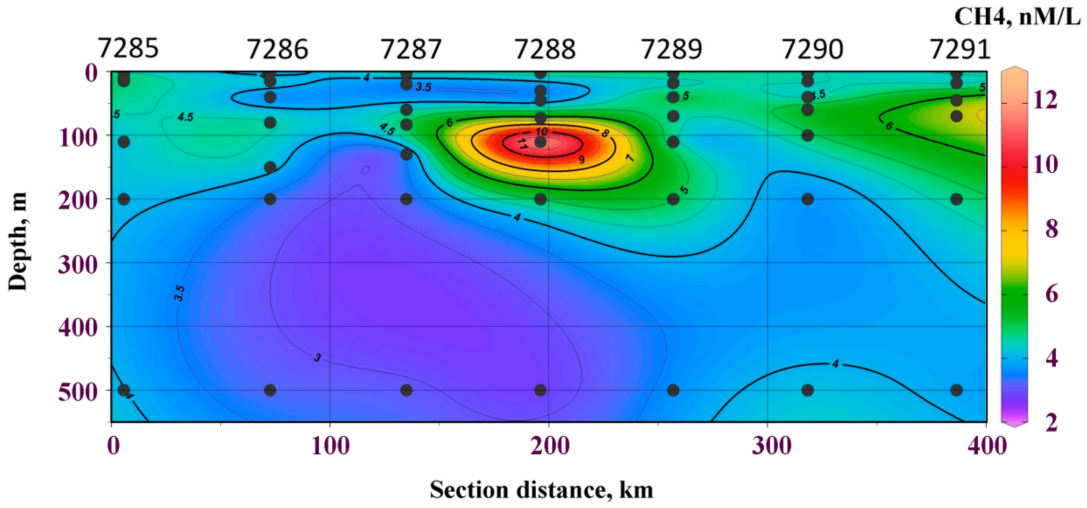


Figure 10. Distribution of methane concentration over the section.

3.4. Biooptics

Studies over a section in the rings made it possible to reveal some features of the vertical distribution of biooptical parameters (Figure 11). In the anticyclonic eddy, the depth of the maximum concentration of chlorophyll-a (deep chlorophyll maximum, DCM) was 70–80 m, which is deeper compared to the cyclonic eddy, where DCM varied in the range of 45–60 m (Figure 11a). At stations located closer to the centers of the rings, the deepest DCMs were found (station 7286, ~80 m) in the anticyclonic eddy, and the least deep ones were in the cyclone (station 7290, ~45 m). This was caused by velocities directed downward in the central part of the anticyclonic eddy and upward in the central part of the cyclonic eddy. In both cases, the vertical velocities increase towards the center of the rings.

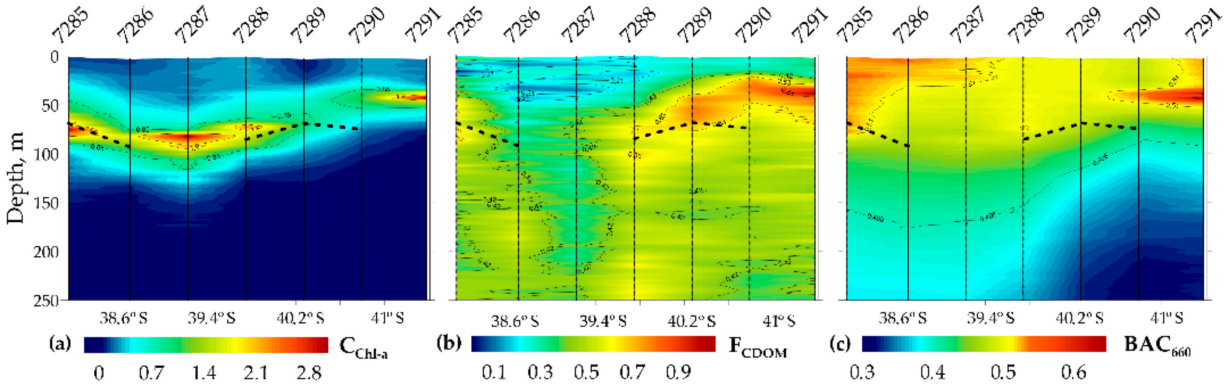


Figure 11. Section of chlorophyll "a" concentration (C_{chl-a}, μg/L) (**a**), fluorescence intensity of colored dissolved organic matter (FCDOM, QSU) (**b**) and directional light attenuation index (BAC660, FTU) (**c**); Dashed black lines on the sections mark the depth of the photic zone (Zeu).

One can see on the C_{chl-a} section (Figure 11a) that in the anticyclonic eddy the width of the peak on the vertical profile of C_{chl-a} is greater than in the cyclonic eddy (50–70 m and 30–50 m, respectively). This is due to large vertical density gradients in the seasonal pycnocline in the central part of the cyclonic ring compared to the anticyclonic ring. High values of vertical density gradients are a barrier to the vertical motion of phytoplankton cells, nutrients, and other suspended and dissolved substances [51–53], which leads to an increase in the concentration of substances in the seasonal pycnocline. This is the reason for the appearance of pronounced layers of increased FCDOM and BAC660 values, and a

decrease in the width of the $C_{chl\text{-}a}$ peak in the pycnocline of the central part of the cyclonic ring, which can be seen in the vertical sections of these parameters (Figure 11).

Despite the previously shown differences in the vertical distributions of $C_{chl\text{-}a}$, the maximum values of $C_{chl\text{-}a}$ in the anticyclonic and cyclonic rings were approximately the same and reached 3 µg/L. However, the maximum values of other biooptical characteristics (FCDOM and BAC660) were different.

The vertical distribution of FCDOM (Figure 11b) differs significantly in the two rings. In the upper mixed layer (UML) of the anticyclonic ring, the mean FCDOM values are lower than those in the underlying layers. At the same time, in the center of the anticyclonic ring, there is a zone of water deepening up to 220 m with reduced FCDOM values (St. 7286, 7287). In the cyclonic ring, within the UML, the minimum values of FCDOM were also observed, and the maximum values, similar to the $C_{chl\text{-}a}$ distributions, were found in the pycnocline. In the layer below the pycnocline up to the maximum sounding depth, FCDOM almost does not change with depth (0.4–0.5 QSU). In the cyclonic ring, the average FCDOM values are higher in each of the layers compared to the values in the anticyclonic ring.

The vertical distribution of BAC660 (Figure 11c) revealed common patterns with the distribution of $C_{chl\text{-}a}$ but some differences were found. In the anticyclonic ring, waters with elevated BAC660 values, such as Cchl-a, deepen in the central part of the ring. However, in the vertical distribution of BAC660 there is no pronounced deepened local maximum, as in the case of Cchl-a. In the anticyclonic ring, the BAC660 values decreased monotonously with depth from 0.55 FTU at the surface to 0.4 FTU at a depth of 250 m. In the cyclonic ring, the vertical profile of BAC_{660} is similar to that of $C_{chl\text{-}a}$. Namely, BAC660 slightly changes in the UML; it has a maximum in the seasonal pycnocline of about 0.7 FTU, decreases below the pycnocline to 0.4 FTU at depths of 90–110 m and further to a minimum value of 0.3 FTU at a depth of 250 m. The absolute maximum the BAC660 value was observed in the pycnocline of the central part of the cyclonic ring, similar to the FCDOM distribution.

Based on underwater PAR measurements, the depth of the photic zone (Zeu) was determined as 1% of the PAR incident on the sea surface. The Zeu estimates in the section ranged from 69 to 93 m and are marked as dotted black lines in Figure 11a,c. At night stations 7287 and 7291, Zeu data are not available. In the presented data, Zeu was determined from the total effect on light attenuation of TSM (Figure 11c) and CDOM (Figure 11b).

These features of the vertical distribution of biooptical characteristics indicate that anticyclonic eddies manifest themselves on the satellite images on the color of the ocean as areas with low chlorophyll-a concentrations, and cyclonic eddies appear as areas with increased chlorophyll-a concentrations [21,27]. This is due not only to the chlorophyll-a concentration, but also to the DCM value, and the content of additional TSM or CDOM [54].

3.5. Primary Production

The primary productivity of phytoplankton (i.e., photosynthetic ability) is determined by three main factors: the amount of the main photopigment chlorophyll "a", the amount of available light energy, and the amount of nutrients (the material basis of photosynthesis). Analysis of the distribution of these factors over the section revealed certain differences.

The total content of chlorophyll "a" (extract method) in the euphotic layer showed a uniform distribution over water masses (45.4–83.9 mg/m^2) (Figure 12a) with a maximum content at the northern periphery of the anticyclonic ring (station 7285). The integral primary production in the cold cyclonic ring was more than twice as high as in the subtropical one (on average 155.8 and 72.0 mgC/m^2 per day, respectively) (Figures 12 and 13). Distributions of the total content of chlorophyll "a" and the integral primary production in Figure 12 show that the maximum of integral primary production and high chlorophyll "a" content occur in the frontal zone between the rings, i.e., between stations 7288 and 7289. The area of increased primary productivity correlates with the high nutrient content.

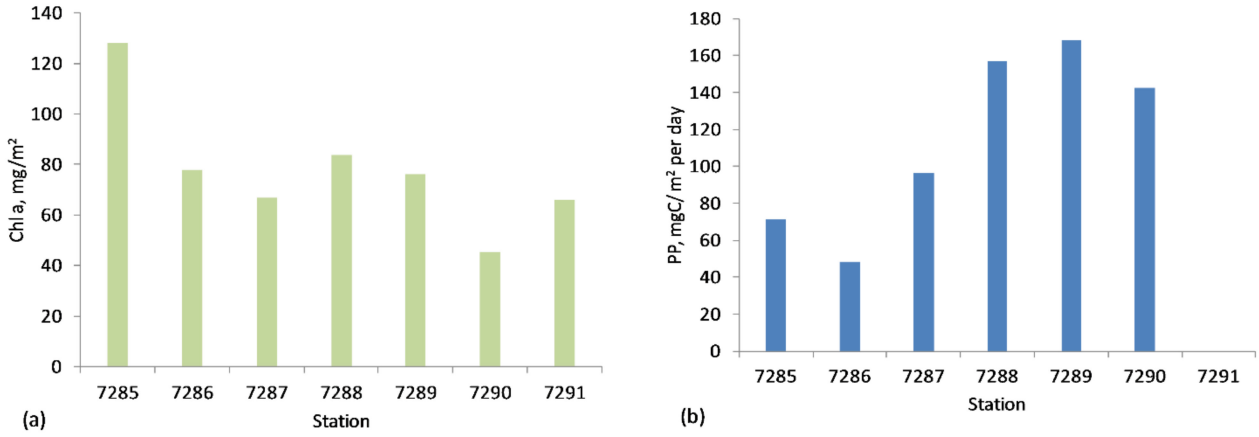


Figure 12. Distribution of the total content of chlorophyll "a" (determined by the extract method) (**a**) and the integral primary production (**b**) in the euphotic layer in the section.

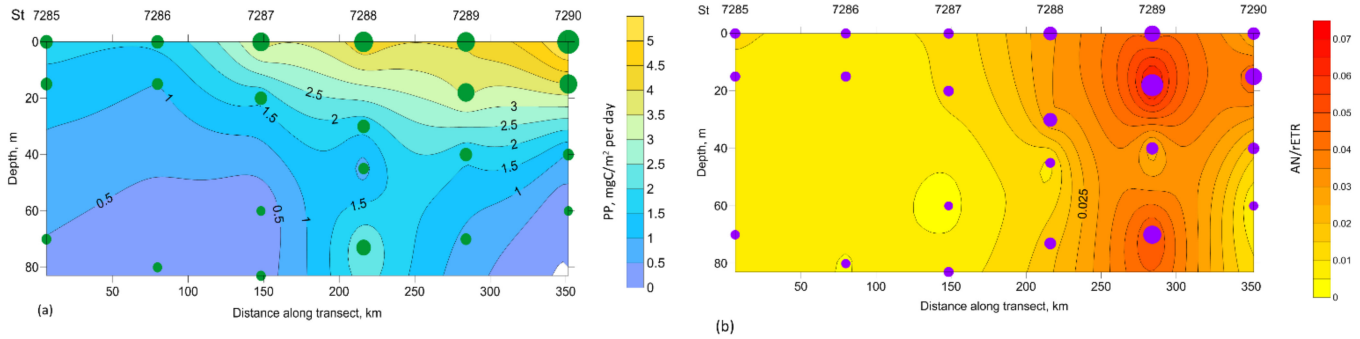


Figure 13. Spatial distribution of primary production (**a**) and photosynthetic efficiency (**b**) of phytoplankton in the euphotic layer. Circles indicate the location of sampling points, and their size is proportional to the values of the corresponding parameter.

The observed distribution of high values of primary production in this water mass is caused by high density stratification in the center of the eddy in the upper zone of the euphotic layer, which retains phytoplankton. In addition, the upward vertical velocity in the central part of the cyclonic (Subantarctic) eddy apparently promotes upwelling of nutrient-rich deep waters into the photosynthesis zone. In the interaction zone, where high velocities were measured, mixing occurs in the euphotic layer, and phytoplankton cells periodically appear in the zones of different illumination. Hence, active phytoplankton occupies the entire thickness of the euphotic layer.

3.6. Invertebrates

The catches of invertebrates at both stations contained elements of both Subantarctic *Primnoa micropa* (Amphipoda) and tropical *Vibia* spp., *Phronima* spp. (Amphipoda) fauna, as well as widespread species *Travisiopsis lanceolata* (Polychaeta). However, elements of tropical fauna prevailed at St. 7286; amphipods Platyscelidae gen. sp., pelagic polychaetes *Lopadorrhynchus appendiculatus*, *L.* cf. *nationalis*, *Rhynchonereella gracilis* and *Torrea candida* were encountered only at this station. St. 7290 was characterized by the predominance of the Subantarctic *Themisto gaudichaudi compressa* (Amphipoda) and the widespread *Nematoscelis megalops* (Euphausiidae) and *Parandania boecki* (Amphipoda). Polychaetes were represented by the large Antarctic species *Vanadis antarctica*, taxa with unclear distribution *Tomopteris* spp. and larvae of the families Amphinomodae, Polynoidae, Terebellidae.

It is hard to overestimate the significant ecological role of cold- and warm-core rings in large scale transport and small-scale transition, and finally biogeographical distribution of certain aquatic organisms supporting regional biodiversity and ecosystem functioning. One

of the specific zooplankton species from the order Euphausiacea—*Nematoscelis megalops* is considered as a "sign" organism of transition regions between the tropical-subtropical and the subpolar waters in the Atlantic, Pacific, and Indian Oceans [55,56]. There are fragmental observations on *N. megalops* in the Malvinas and the Brazil Currents [57]. Thus, there is lack of information to discuss the comprehensive zoogeography in the SW Atlantic region. In our study, it was found that *N. megalops* was highly abundant in Subantarctic waters of cold-core water ring of the Malvinas Current. In contrast, this species was negligible in subtropical waters of warm-core water ring of the Brazil Current. Our record of *N. megalops* testifies to the selection of preferable water column and water properties by this species to maintain trophic and reproduction demands. It is known that *N. megalops* is able to occupy a depth from 800 m up to the surface layers but generally occurs at the depths from 300 to 600 m at favored temperatures ranging 8–10 °C [58,59]. Indeed, *N. megalops* was collected by us in a steam of cold-core water ring at depths from 640 m to the surface, within the preferable temperature range.

We noted that the occurrence and abundance of *N. megalops* were associated with the presence of top predators such as baleen whales (Mysticeti) and, in particular, the sei whale *Balaenoptera borealis*. According to our observations, eight sei whales were found in the cold-core water ring of the Malvinas Current. It is known that sei whales feed on zooplankton. Euphausiids are one of the major food items [60,61].

Moreover, our further studies will be focused on ecological and biochemical characteristics based on lipid and energetic status investigations of *N. megalops* in the studied area to determine general and specific patterns of euphausiids associated with environmental variables.

3.7. Ichthyoplankton

Species composition of ichthyoplankton samples at both stations considerably differed (Table 2). At St. 7286, warm water species distributed mostly in tropical and subtropical waters were caught, while the catch at St. 7290 was represented mainly by species occurring as a rule in cold waters of the notal zone, Subantarctic, and Antarctic. At the same time, *Cyclothone* spp. were found in both rings but more frequently within the warm waters of the Brazil Current.

Table 2. Species composition of ichthyoplankton at different stations.

Fish Taxa	Range Type (Source)	Number of Specimens(Fry/Larvae)	
		St. 7286	St. 7290
	Phosichthyidae		
Phosichthys argenteus	Subtropical-Notal [62]	19/1	0
	Sternoptychidae		
Argyropelecus hemigymnus	Temperate-subtropical [63]	3/17	0
Sternoptyx diaphana	Tropical-subtropical [64]	0/1	0
	Stomiidae		
Chauliodus schmidti	Tropical [65]	3/0	0
	Gonostomatidae		
Cyclothone braueri	Temperate-subtropical [63]	52/10	6/0
C. pseudopallida	Temperate-subtropical [63]	3/0	4/0
Cyclothone spp.	Not applicable	18/0	0

Table 2. *Cont.*

Fish Taxa	Range Type (Source)	Number of Specimens(Fry/Larvae)	
		St. 7286	St. 7290
Myctophidae			
Diogenichthys atlanticus	Temperate-subtropical [63]	0/11	0
Krefftichthys anderssoni	Notal-Antarctic [43]	0	0/4
Protomyctophum normani	Notal [43]	0	0/14
P. bolini	Notal-Antarctic [43]	0	04
Hygophum bruni	Subantarctic [43]	0	0/2
H. hanseni	Notal [43]	0	0/2
Diaphus anderseni	Tropical-subtropical [43]	0	0/2
Diaphus sp.	Not applicable	0	0/1
Lampanyctus sp.	Not applicable	2/0	0
Fish larvae (inident.)	Not applicable	18	0

3.8. Sea Mammals and Birds

Two species of sea mammals and eight of the most numerous species of birds were recorded in the rings (Table 3).

Table 3. Species composition (number of individuals observed) of sea mammals and birds in the rings.

Species	Subtropical Water	Subantarctic Water	Frontal Zone
Sea Mammals			
Sei whale *Balaenoptera borealis*	0	8	0
Southern bottlenose whale *Hyperoodon planifrons*	3	0	0
Sea Birds			
Spectacled petrel *Procellaria conspicillata*	81	29	25
Soft-plumaged petrel *Pterodroma mollis*	78	17	13
Atlantic petrel *Pterodroma incerta*	16	7	5
Cory's shearwater *Calonectris diomedea*	5	9	7
White-chinned petrel *Procellaria aequinoctialis*	2	54	23
Great shearwater *Ardenna gravis*	1	24	12
Atlantic yellow-nosed albatross. *Thalassarche chlororhynchos*	7	5	5
Wandering albatross. *Diomedea exulans*	2	10	7
Albatross sp. *Diomedeidae* sp.	2	8	4

Marine mammals occurred in both rings. In the ring of subtropical water, three southern bottlenose whales (*Hyperoodon planifrons*) were recorded. At the same time, toothed whales were not found in Subantarctic waters, while eight sei whales were (*Balaenoptera borealis*) sighted in the ring. It is known that these two species have completely different trophic ecologies. The southern bottlenose whale has a circumpolar distribution in the southern hemisphere (south of 30° S). This species is most common in the region of 57–70° S probably migrating to Antarctica in summer. The southern bottlenose is characterized

by feeding at great depths exceeding 1000 m, mainly on squid, but also on fish, such as Patagonian toothfish *Dissostichus eleginoides*. The sei whale is distributed from the tropical to the circumpolar zone in both hemispheres, mainly found in the open ocean far from the coast. The main food of the sei whale is zooplankton and small fish [60].

The majority of birds encountered in the areas of the two rings were represented by two families: albatrosses (Diomedeidae), and petrels (Procellariidae). It was found that the petrel family was the most numerous and diverse in terms of species composition (Table 3). However, a change in the occurrence of some species was noted during the transition from the anticyclonic ring to the cyclonic ring (Figure 14). For example, the number of spectacled petrel (*Procellaria conspicillata*), a mass bird species in the subtropical area, was 81 individuals, while their number decreased by almost three times in Subantarctic water (29 individuals). A decrease in the number of occurrences during the transition from subtropical to Subantarctic waters was also characteristic of the soft-fin typhoon (Pterodroma mollis) and Atlantic petrel (*P. incerta*): from 78 individuals to 17 individuals, and from 16 individuals to 7 individuals, respectively.

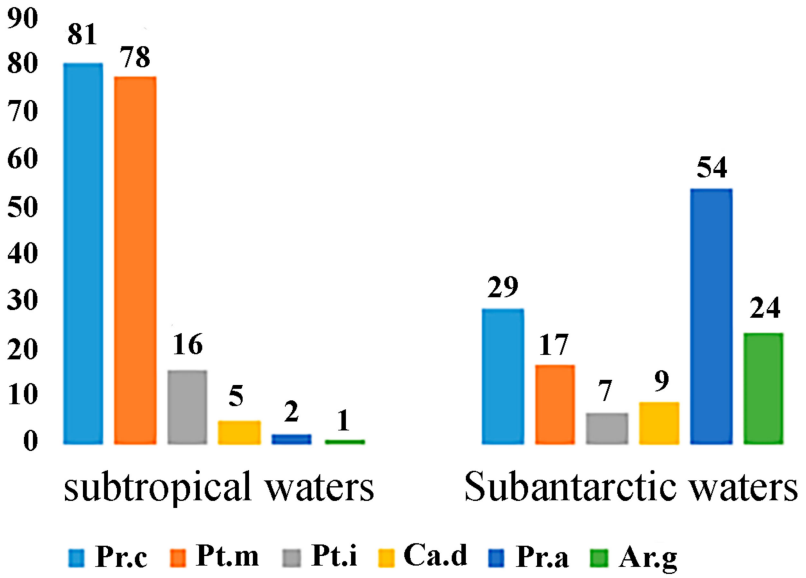


Figure 14. The Procellariidae family in the region of rings. Note: Pr.c is the spectacled petrel *Procellaria conspicillata*, Pt.m is the soft-plumaged petrel *Pterodroma mollis*, Pt.i is the Atlantic petrel *Pterodroma incerta*, Ca.d is Cory's shearwater *Calonectris diomedea*, Pr.a is the white-chinned petrel *Procellaria aequinoctialis*, Ar.g is the great shearwater *Ardenna gravis*.

On the contrary, some species of this family, when moving from one ring to another, began to occur much more frequently. For example, the white-chinned petrel (*Procellaria aequinoctialis*) was the most abundant bird species in the ring of Subantarctic water, 54 individuals, while this species was recorded only two times in the ring of subtropical water. An increase in occurrence in the ring of Subantarctic waters was noted for the gray petrel (*Ardenna gravis*) and Cory's shearwater (*Calonectris Diomedea*): from 1 to 24 individuals and from 5 to 9 individuals, respectively.

A change in the occurrence of some species of the albatross family during the transition from subtropical to Subantarctic waters was observed. This family was more numerous in the area of the Subantarctic ring. The wandering albatross (*Diomedea exulans*) was found five times more often in the Subantarctic ring than in subtropical waters.

Marine life at oceanic fronts is an interesting oceanographic object. Frontal zones are known as regions with favorable conditions for feeding of different species including pelagic fish, mammals and birds. A review of marine life at oceanic fronts is given in [66].

A frontal zone was found in the interval between stations 7287–7291. Marine mammals were not observed here. Most of the birds encountered in Subantarctic waters were found

in this narrow frontal region (Table 3). Starting from the frontal zone, the number of some species of birds began to increase compared to in the subtropical water. The number of birds found in the frontal zone increased towards the cold ring. This increase was recorded for some petrels and the great shearwater (*Ardenna gravis*) (Table 3).

Based on the results of observations, we conclude that marine mammals and some species of birds were more common in the cyclonic ring; however, other species of birds were more common in the anticyclonic one. Some species of birds were common in the frontal zone and their numbers increased towards the cold ring. At the same time, the species composition and abundance of both marine mammals and birds in these two areas differed, indicating that these animals are confined to the conditions of their habitat.

4. Summary

We analyzed the properties of sea water in two intense rings of the South Atlantic in the region of the Brazil–Malvinas Confluence. One ring separated from the Brazil Current and the other from the Malvinas Current. Analysis is based on the CTD casts, ADCP measurements from onboard velocity profiler. The properties of subtropical and Subantarctic seawater were strongly different and a strong current was recorded at the interface between rings. Backward-in-time Lagrangian analysis revealed that waters of various origin from various surrounding regions were entrained in the rings. Analysis of different properties was supplemented by investigation of optical properties and chemical parameters such as dissolved oxygen, nitrates, silicates, pH and methane concentration. We also studied different biological properties in the rings such as primary production, plankton, fish, and invertebrates. The catches revealed different concentrations and species of plankton and other invertebrates. Analysis of the strong differences between the rings is supplemented by observations of whales and birds in the region.

Author Contributions: E.G.M., D.I.F.: Conceptualization, original draft preparation, writing, and editing; V.A.K., O.A.Z., O.S.M.: physical oceanography part; A.A.L., P.A.S., E.A.S.: optical part; A.A.K., M.V.B., V.I.P.: Lagrangian model; A.M.S., A.L.C., A.V.M. (Anna V. Masevich), N.I.T.: chemical part; A.M.O., S.A.M. (Svetlana A. Murzina), A.V.M. (Alexej V. Mishinand), N.Y.N., G.D.K., V.L.S.: biological parts; S.A.M. (Sergey A. Mosharovand), I.V.M.: primary production; A.O.K.: methane; P.V.C., A.V.T., L.G.T., A.D.C.; mammals and birds. All authors have read and agreed to the published version of the manuscript.

Funding: Ship measurements were supported by the targeted financial support from the Ministry of Science and Higher Education of the Russian Federation: State Tasks FMWE-2022-0001 (SIO), FNNN-20222-0001 (MHI), 0211-2019-0007 (POI), FFER-2019-0021 (IPEE), and Russian Science Foundation (ship operation, grant no. 21-77-2004).

Informed Consent Statement: No studies involving humans were performed. Birds and mammals were observed using binoculars and photo cameras. No experiments with animals have been carried out.

Data Availability Statement: Data are available upon request.

Conflicts of Interest: The authors declare no conflict of interest.

References

1. Kamenkovich, V.M.; Koshlyakov, M.N.; Monin, A.S. *Synoptic Eddies in the Ocean*; Springer: Berlin/Heidelberg, Germany, 1986; p. 444.
2. Stammer, D.; Wunsch, C. Temporal changes in eddy energy of the oceans. *Deep-Sea Res. I* **1999**, *46*, 77–108. [CrossRef]
3. Olson, D.B. Rings in the ocean. *Annu. Rev. Earth Planet. Sci.* **1991**, *19*, 283–311. [CrossRef]
4. Gordon, A.L.; Greengrove, C.L. Geostrophic circulation of the Brazil-Falkland confluence. *Deep-Sea Res. I* **1986**, *33*, 573–585. [CrossRef]
5. Orúe-Echevarría, D.; Pelegrí, J.L.; Alonso-González, I.J.; Benítez-Barrios, V.M.; Emelianov, M.; García-Olivares, A.; Rubinat, M.G.; De La Fuente, P.; Herrero, C.; Isern-Fontanet, J.; et al. A view of the Brazil-Malvinas confluence, March 2015. *Deep–Sea Res. I* **2021**, *172*, 103533. [CrossRef]

6. Valla, D.; Piola, A.R. Evidence of upwelling events at the northern Patagonian shelf break. *J. Geophys. Res. Oceans* **2015**, *120*, 7635–7656. [CrossRef]
7. Frey, D.I.; Piola, A.R.; Krechik, V.A.; Fofanov, D.V.; Morozov, E.G.; Silvestrova, K.P.; Tarakanov, R.Y.; Gladyshev, S.V. Direct measurements of the Malvinas Current velocity structure. *J. Geophys. Res. Oceans* **2021**, *126*, e2020JC016727. [CrossRef]
8. Piola, A.R.; Franco, B.C.; Palma, E.D.; Saraceno, M. Multiple jets in the Malvinas Current. *J. Geophys. Res. Oceans* **2013**, *118*, 2107–2117. [CrossRef]
9. Artana, C.; Provost, C.; Poli, L.; Ferrari, R.; Lellouche, J.-M. Revisiting the Malvinas Current upper circulation and water masses using a high-resolution ocean reanalysis. *J. Geophysical Res. Oceans* **2021**, *126*, e2021JC017271. [CrossRef]
10. Barré, N.; Provost, C.; Saraceno, M. Spatial and temporal scales of the Brazil–Malvinas Current confluence documented by simultaneous MODIS Aqua 1.1-km resolution SST and color images. *Adv. Space Res.* **2006**, *37*, 770–786. [CrossRef]
11. Gordon, A.L. Brazil-Malvinas Confluence–1984. *Deep Sea Res. Part. A* **1989**, *36*, 359–384. [CrossRef]
12. Garcia, C.A.; Sarma, Y.; Mata, M.M.; Garcia, V.M. Chlorophyll variability and eddies in the Brazil–Malvinas Confluence region. *Deep Sea Res. II* **2004**, *51*, 159–172. [CrossRef]
13. Jullion, L.; Heywood, K.J.; Naveira Garabato, A.C.; Stevens, D.P. Circulation and water mass modification in the Brazil–Malvinas Confluence. *J. Phys. Oceanogr.* **2010**, *40*, 845–864. [CrossRef]
14. Manta, G.; Speich, S.; Karstensen, J.; Hummels, R.; Kersalé, M.; Laxenaire, R.; Meinen, C.S. The South Atlantic Meridional Overturning Circulation and Mesoscale Eddies in the First GO-SHIP Section at 34.5° S. *J. Geophys. Res. Oceans* **2021**, *126*, e2020JC016962. [CrossRef]
15. Valla, D.; Piola, A.R.; Meinen, C.S.; Campos, E. Strong mixing and recirculation in the northwestern Argentine Basin. *J. Geophys. Res. Oceans* **2018**, *123*, 4624–4648. [CrossRef]
16. Manta, G.; Speich, S.; Barreiro, M.; Trinchin, R.; de Mello, C.; Laxenaire, R.; Piola, A.R. Shelf water export at the Brazil-Malvinas Confluence evidenced from combined in-situ and satellite observations. *Front. Mar. Sci.* **2022**, *9*, 857594. [CrossRef]
17. Meinen, C.S.; Speich, S.; Perez, R.C.; Dong, S.; Piola, A.R.; Garzoli, S.L.; Baringer, M.O.; Gladyshev, S.; Campos, E.J.D. Temporal variability of the meridional overturning circulation at 34. *5○S: Results from two pilot boundary arrays in the South Atlantic. J. Geophys. Res. Oceans* **2013**, *118*, 6461–6478. [CrossRef]
18. Lumpkin, R.; Garzoli, S. Interannual to decadal changes in the western South Atlantic's surface circulation. *J. Geophys. Res. Oceans* **2011**, *116*, C01014. [CrossRef]
19. Artana, C.; Provost, C.; Lellouche, J.-M.; Rio, M.-H.; Ferrari, R.; Sennéchael, N. The Malvinas Current at the confluence with the Brazil Current: Inferences from 25 years of Mercator Ocean reanalysis. *J. Geophys. Res. Oceans* **2019**, *124*, 7178–7200. [CrossRef]
20. Matano, R.P.; Combes, V.; Piola, A.R.; Guerrero, R.; Palma, E.D.; Strub, P.T.; James, C.; Fenco, H.; Chao, Y.; Saraceno, M. The salinity signature of the cross-shelf exchanges in the Southwestern Atlantic Ocean: Numerical simulations. *J. Geophys. Res. Oceans* **2014**, *119*, 7949–7968. [CrossRef]
21. Gaube, P.; Barceló, C.; McGillicuddy, D.J., Jr.; Domingo, A.; Miller, P.; Giffoni, B.; Marcovaldi, N.; Swimmer, Y. The use of mesoscale eddies by juvenile loggerhead sea turtles (Caretta caretta) in the southwestern Atlantic. *PLoS ONE* **2017**, *12*, e0172839. [CrossRef]
22. Lentini, C.A.D.; Olson, D.B.; Podestá, G.P. Statistics of Brazil Current rings observed from AVHRR: 1993 to 1998. *Geophys. Res. Lett.* **2002**, *29*, 1811. [CrossRef]
23. Lentini, C.A.D.; Goni, G.J.; Olson, D.B. Investigation of Brazil Current rings in the confluence region. *J. Geophys. Res. Oceans* **2006**, *111*, C06013. [CrossRef]
24. Mason, E.; Pascual, A.; Gaube, P.; Ruiz, S.; Pelegrí, J.L.; Delepoulle, A. Subregional characterization of mesoscale eddies across the Brazil-Malvinas Confluence. *J. Geophys. Res. Oceans* **2017**, *122*, 3329–3357. [CrossRef]
25. Frenger, I.; Münnich, M.; Gruber, N.; Knutti, R. Southern Ocean eddy phenomenology. *J. Geophys. Res. Oceans* **2015**, *120*, 7413–7449. [CrossRef]
26. Chelton, D.B.; Schlax, M.G.; Samelson, R.M.; de Szoeke, R.A. Global observations of large oceanic eddies. *Geophys. Res. Lett.* **2007**, *34*, L15606. [CrossRef]
27. Saraceno, M.; Provost, C. On eddy polarity distribution in the southwestern Atlantic. *Deep Sea Res. I* **2012**, *69*, 62–69. [CrossRef]
28. Willson, H.R.; Rees, N.W. Classification of mesoscale features in the Brazil-Falkland Current confluence zone. *Prog. Oceanogr.* **2000**, *45*, 415–426. [CrossRef]
29. Wessel, P.; Smith, W.H.F. A global, self-consistent, hierarchical, high-resolution shoreline database. *J. Geophys. Res.* **1996**, *101*, 8741–8743. [CrossRef]
30. Pujol, M.-I.; Faugère, Y.; Taburet, G.; Dupuy, S.; Pelloquin, C.; Ablain, M.; Picot, N. DUACS DT2014: The new multi-mission altimeter data set reprocessed over 20 years. *Ocean. Sci.* **2016**, *12*, 1067–1090. [CrossRef]
31. Prants, S.V. Backward-in-time methods to simulate large-scale transport and mixing in the ocean. *Phys. Scr.* **2015**, *90*, 074054. [CrossRef]
32. Chereskin, T.K.; Harris, C.L. *Shipboard Acoustic Doppler Current Profiling during the WOCE Indian Ocean. Expedition*; Scripps Institution of Oceanography, University of California: San Diego, CA, USA, 1997; Volume 10, p. 137.
33. Egbert, G.D.; Erofeeva, S.Y. Efficient inverse modeling of barotropic ocean tides. *J. Atmosph. Oceanic Tech.* **2002**, *19*, 183–204. [CrossRef]
34. Vereshchagina, O.F.; Korovitskaya, E.V.; Mishukova, G.I. Methane in water columns and sediments of the north western Sea of Japan. *Deep-Sea Res. II* **2013**, *86*, 25–33. [CrossRef]

35. Yamamoto, S.; Alcauskas, J.B.; Crozier, T.E. Solubility of methane in distilled water and sea water. *J. Chem. Eng. Data* **1976**, *21*, 78–80. [CrossRef]
36. Wiesenburg, D.A.; Guinasso, N.L. Equilibrium solubility of methane, carbon monooxide, and hydrogen in water and sea water. *J. Chem. Eng. Data* **1979**, *24*, 356–360. [CrossRef]
37. Jerlov, N.G. *Marine Optics*, 2nd ed.; Elsevier Oceanography Series: Amsterdam, The Netherlands, 1976; Volume 14, p. 371.
38. JGOFS (Joint Global Ocean Flux Study Protocols). *Protocols for the Joint Global Ocean Flux Study Protocols (JGOFS) Core Measurements*; UNESCO: Paris, France, 1994; pp. 119–122.
39. Steemann-Nielsen, E. The use of radio-active carbon (C14) for measuring organic production in the sea. *J. Cons. /Cons. Perm. Int. L'exploration Mer.* **1952**, *18*, 117–140. [CrossRef]
40. Genty, B.; Briantais, J.-M.; Baker, N.R. The relationship between the quantum yield of photosynthetic electron transport and quenching of chlorophyll fluorescence. *Biochim. Biophys. Acta* **1989**, *990*, 87–92. [CrossRef]
41. Schreiber, U. Pulse amplitude (PAM) fluorometry and saturation pulse method: An overview. In *Chlorophyll a Fluorescence: A Signature of Photosynthesis*; Advances in Photosynthesis and Respiration Series; Papageorgiou, G., Govindjee, G., Eds.; Kluwer Academic Publishers: Dordrecht, Germany, 2004; pp. 270–319.
42. Bouchard, C.; Mollard, S.; Suzuki, K.; Robert, D.; Fortier, L. Contrasting the early life histories of sympatric Arctic gadids Boreogadus saida and Arctogadus glacialis in the Canadian Beaufort Sea. *Pol. Biol.* **2016**, *39*, 1005–1022. [CrossRef]
43. Becker, V.E. *Miktofovye Ryby Mirovogo Okeana (Myctophid Fish of the World Ocean)*; Nauka: Moscow, Russia, 1983; p. 246.
44. Moser, H.G.; Ahlstrom, E.H. The role of larval stages in systematic investigations of marine teleosts: The Myctophidae, a case study. In *The Early Life History of Fish*; Springer: Berlin/Heidelberg, Germany, 1974; pp. 605–607.
45. Olivar, M.P.; Fortuño Alós, J.M. Guide to ichthyoplankton of the Southeast Atlantic (Benguela Current region). *Sci. Mar.* **1991**, *55*, 1–383.
46. Pertseva-Ostroumova, T.A. Some morphological characteristics of myctophid larvae (Myctophidae, Pisces). Fishes of the Pacific and Indian Oceans, biology and distribution. *Tr. Inst. Okeanol. Akad. Nauk SSSR* **1964**, *73*, 79–97.
47. Richards, W.J. *Early Stages of Atlantic Fishes: An Identification Guide for the Western Central North Atlantic*; CRC Press: Boca Raton, FL, USA, 2006; p. 1824.
48. Sutton, T.T.; Hulley, P.A.; Wienerroither, R.; Zaera-Perez, D.; Paxton, J.R. *Identification Guide to the Mesopelagic Fishes of the Central and South East Atlantic Ocean*; FAO: Rome, Italy, 2020; p. 346. [CrossRef]
49. Ponomarev, V.I.; Fayman, P.A.; Prants, S.V.; Budyansky, M.V.; Uleysky, M.Y. Simulation of mesoscale circulation in the Tatar Strait of the Japan Sea. *Ocean Model.* **2018**, *126*, 43–55. [CrossRef]
50. Prants, S.V.; Budyansky, M.V.; Uleysky, M.Y. Lagrangian simulation and tracking of the mesoscale eddies contaminated by Fukushima-derived radionuclides. *Ocean Sci.* **2017**, *13*, 453–463. [CrossRef]
51. Davis, K.; Anderson, M.A.; Yates, M.V. Distribution of indicator bacteria in Canyon Lake, California. *Water Res.* **2005**, *39*, 1277–1288. [CrossRef] [PubMed]
52. Elci, S. Effects of thermal stratification and mixing on reservoir water quality. *Limnology* **2008**, *9*, 135–142. [CrossRef]
53. Latushkin, A.A.; Artamonov, Y.V.; Lee, R.I.; Sysoev, A.A.; Sysoeva, I.V.; Fedirko, A.V.; Martynov, O.V. The Northern Part of the Black Sea Waters' Bio-optical and Hydrology Structure Features in the Autumn Period 2016. *Fundam. I Prikl. Gidrofiz.* **2020**, *13*, 78–82. [CrossRef]
54. Lipinskaia, N.A.; Salyuk, P.A. Analysis of Hydro-Biological and Hydro-Optical Characteristics in Submesoscale Eddies in the Gulf of Peter the Great with the Use of Simultaneous in-situ and Remote Measurements. *Fundam. Appl. Hydrophys.* **2021**, *14*, 111–121. (In Russian) [CrossRef]
55. Barange, M.; Gibbons, M.J.; Carola, M. Diet and feeding of Euphausia hanseni and Nematoscelis megalops (Euphausiacea) in the northern Benguela Current: Ecological significance of vertical space partitioning. *Mar. Ecol. Prog. Ser.* **1991**, *73*, 173–181. [CrossRef]
56. Wiebe, P.H.; Boyd, S.H. Limits of Nematoscelis megalops in the Northwestern Atlantic in relation to Gulf Stream cold core rings. I. Horizontal and vertical distributions. *J. Mar. Res.* **1978**, *36*, 119–142.
57. Curtulo, L.M.; Dadon, J.R.; Mazzoni, H.E. Distribution and abundance of euphausiids off Argentina in spring 1978. *Neritica* **1990**, *5*, 1–14.
58. Werner, T.; Huenerlage, K.; Verheye, H.; Buchholz, F. Thermal constraints on the respiration and excretion rates of krill, Eupausia hanseni and Nematoscelis megalops, in the northern Benguela upwelling system off Namibia. *Afr. J. Mar. Sci.* **2012**, *34*, 391–399. [CrossRef]
59. Yoon, W.D.; Nival, P.; Choe, S.A.; Picheral, M.; Gorsky, G. Vertical distribution and nutritional behavior of Cyclothone braueri, Nematoscelis megalops, Meganyctiphanes norvegica and Salpa fusiformis in the NW Mediterranean mesopelagic zone. *ICES CM F* **2007**, *3*, 1–28.
60. Jefferson, T.A.; Webber, M.A.; Pitman, R.L. Marine Mammals of the World. In *A Comprehensive Guide to Their Identification*; Elsevier: Amsterdam, The Netherlands, 2015; 608p.
61. Kawamura, A. A review of food of Balaenopterid whales. *Sci. Rep. Whales Res. Inst.* **1980**, *32*, 155–197.
62. Balushkin, A.V. Findings of the silver lightfish Phosichthys argenteus (Phosichthyidae) at the Pulkovo Ridge (South-Central Pacific). *J. Ichthyol.* **2017**, *57*, 821–826. [CrossRef]

63. Porteiro, F.M.; Sutton, T.T.; Byrkjedal, I.; Orlov, A.M.; Heino, M.; Menezes, G.; Bergstad, O.A. Fishes of the Northern Mid-Atlantic Ridge collected during the MAR-ECO cruise in June–July 2004: An annotated checklist. Arquipel. *Life Mar. Sci.* **2017**, *10*, 126.
64. Weitzman, S.H. Family No. 75: Sternoptychidae. In *Smiths' Sea Fishes*; Smith, M.M., Heemstra, P.C., Eds.; J.L.B. Smith Institute of Ichthyology: Grahamstown, South Africa, 1986; pp. 253–259.
65. Ege, V. Chauliodus Schn., bathypelagic genus of fishes. A systematic, phylogenetic and geographical study. *Dana Rep.* **1948**, *31*, 1–146.
66. Prants, S.V. Marine life at Lagrangian fronts. *Prog. Oceanogr.* **2022**, *204*, 102790. [CrossRef]